

On the Performance Evaluation of 5G MIMO Networks employing NOMA via System-Link Level Simulations

P. Gkonis, P. Trakadas, L. Sarakis

General Department
National and Kapodistrian University of Athens
Sterea Ellada, 34400 Dirfies Messapies, Greece
e-mails: {pgkonis,ptrakadas,lsaralis} @uoa.gr

A. Giannopoulos, S. Spantideas, N. Capsalis

National Technical University of Athens
9, Iroon Polytechniou str., Athens, 15780, Greece
e-mails: angianno@mail.ntua.gr,
sspantideas@central.ntua.gr, ncapsalis@gmail.com

Abstract—In this paper the performance of a proposed non-orthogonal multiple access (NOMA) scheme in a fifth-generation (5G) multicellular orientation is evaluated. To this end, a hybrid system-link level simulator has been developed, making the performance evaluation of 5G orientations feasible for various radio resource management strategies. In particular, simulations were performed for a two-tier cellular network (i.e., 57 active sectors) and multiple antennas at both transmission ends (multiple input multiple output - MIMO configuration). According to the presented results, considering a 2×2 MIMO configuration, the total network throughput can be significantly increased when NOMA is employed, without any mean bit error rate (BER) deterioration compared to orthogonal multiple access (OMA) transmission. Importantly, this improvement is achieved with minimum transceiver complexity since the results were derived without employing successive interference cancellation at the receiver side.

Keywords- 5G; NOMA; MIMO; System and link level simulations; Radio Resource Management

I. INTRODUCTION

Broadband wireless access networks have become a reality for the vast majority of mobile users. In this context, bandwidth demanding applications (i.e., live video streaming) define the transmission framework as well as related technologies that have to be adopted. To this end, the existing fourth generation (4G) wireless cellular networks can already deliver peak data rates up to 100 Mbps to mobile stations (MSs) [1]. This is achieved when transmission takes place over multiple assigned subcarriers per MS (or groups of subcarriers, also known as physical resource blocks – PRBs), using the orthogonal frequency division multiple access (OFDMA) physical layer protocol [2]. In addition, the use of multiple antennas at both transmission ends of a wireless configuration (multiple input multiple output – MIMO) can increase the overall system-wide capacity without additional spectrum requirements [3].

However, the ever-increasing demand for higher data rates in zero latency applications in combination with the already crowded spectrum, drive the technological evolutions towards the design and implementation of new transmission and multiple access schemes. Over the last years, scientific research has primarily focused on deployment aspects for fifth generation (5G) wireless

cellular networks. In this framework, millimeter wave (mmWave) transmission along with massive MIMO architecture have been established as the best candidate enabling technologies for 5G network implementation [4] - [5]. Subsequently, carrier frequencies ranging from 30 GHz up to 300 GHz (with equivalent wavelengths from 10 mm to 1 mm) are adopted, thus leading to large bandwidth channels (i.e., of 2 GHz, 4 GHz, 10 GHz, or even 100 GHz). In addition, non-orthogonal multiple access (NOMA) can further improve the total network capacity without requiring additional spectrum resources [6]. In this principle, a higher number of users than the number of orthogonal resource slots can be supported, with the aid of non-orthogonal resource allocation. This may be realized by employing sophisticated inter-user interference cancellation schemes at the cost of an increased receiver complexity. The prominent NOMA schemes are principally divided into two categories, namely, power-domain (PD) and code-domain (CD) NOMA. In the first case, PD NOMA can serve multiple users in the same time slot, OFDMA subcarrier, or spreading code, and multiple access is realized by allocating different power levels to different users [7]. In the second case (CD-NOMA), multiple access schemes rely on low-density spreading (LDS) and sparse code multiple access (SCMA) [8].

A challenging research field towards NOMA implementation is user pairing, a term that includes all policies and conditions under which two independent users can share the same resource block. In this context, a joint user pairing and power allocation problem is considered in [9] to optimize the achievable sum rate with minimum rate constraint for each user. In [10], the impact of user pairing on the performance of two NOMA systems, i.e., fixed power NOMA (F-NOMA) and cognitive radio NOMA, is outlined. According to the presented results, F-NOMA can offer a larger sum rate than orthogonal multiple access (OMA), and the performance gain of F-NOMA over conventional OMA can be further improved by selecting users whose channel conditions are more distinctive. In [11], the authors propose a NOMA pairing scheme that includes a near user and a far user, whose signals are superposed at the transmitter side, and successive interference cancellation (SIC) is applied to the receiver side. Finally, in [12], the authors investigate the minimum pairing distance which separates the far and near users in order to promote massive connectivity. In this

framework, an analytical expression of the pairing distance threshold assuming a fixed power allocation is derived.

However, all the aforementioned studies, consider either limited number of users or restricted network topologies. The goal of this paper is to evaluate the performance of a user pairing approach (NOMA transmission) in 5G multicellular/multiuser wireless orientations, where PRB reuse is based on performance metrics related both to received signal quality of the potential MS as well as to the total amount of interference that causes to the rest co-channel MSs. For this purpose, a hybrid system- link level simulator has been developed, which couples System-Level (SL) and Link-Level (LL) simulations in the same evaluation snapshot (Monte Carlo – MC simulation): MSs enter the network based on predefined SL criteria (e.g., maximum allowed transmission power, blocking rate, etc.) and then LL simulations take place for all active links. Hence, all related Key Performance Indicators (KPIs) can be directly extracted after a sufficient number of MC simulations.

The rest of this paper is organized as follows. In Section II, channel modelling of 5G wireless orientations according to 3GPP specifications is formulated. In Section III, transceiver procedures in the 5G air interface along with the derivation of output metrics are described. In Section IV, the developed simulator along with the proposed NOMA approach are described. Results are presented in Section V, where the benefits of our proposed approach compared to OMA are highlighted. Finally, concluding remarks and proposals for future work are outlined in Section VI.

The following notation is used in the paper. An italic variable a or A denotes a scalar, whereas boldface lowercase and uppercase variables \mathbf{a} and \mathbf{A} denote vectors and matrices, respectively. Moreover, $\|\mathbf{a}\|_F$ stands for the Frobenius norm of vector \mathbf{a} . A calligraphic variable \mathcal{A} denotes a set. Finally, \mathbf{A}^T and \mathbf{A}^H denote the transpose and conjugate transpose of matrix \mathbf{A} , respectively.

II. MIMO WIRELESS CHANNELS IN 5G NETWORKS

The extension of the widely used 3GPP 3D channel model with various additional modeling components can be found in [13]. To this end, the channel coefficient in a non-line of sight (NLOS) environment for the n^{th} cluster ($1 \leq n \leq N$) between an arbitrary pair of Tx,Rx (q,u) is modelled as a sum of individual channels from M subpaths:

$$H_{u,q,n}^{\text{NLOS}} = \sqrt{\frac{P_n}{M}} \sum_{m=1}^M \begin{bmatrix} F_{rx,u,\theta}(\theta_{n,m,ZOA}, \phi_{n,m,AoA}) \\ F_{rx,u,\phi}(\theta_{n,m,ZOA}, \phi_{n,m,AoA}) \end{bmatrix}^T \begin{bmatrix} \exp(j\Phi_{n,m}^{\theta\theta}) & \sqrt{\kappa_{n,m}^{-1}} \exp(j\Phi_{n,m}^{\theta\phi}) \\ \sqrt{\kappa_{n,m}^{-1}} \exp(j\Phi_{n,m}^{\phi\theta}) & \exp(j\Phi_{n,m}^{\phi\phi}) \end{bmatrix} \begin{bmatrix} F_{tx,q,\theta}(\theta_{n,m,ZoD}, \phi_{n,m,AoD}) \\ F_{tx,q,\phi}(\theta_{n,m,ZoD}, \phi_{n,m,AoD}) \end{bmatrix} \exp\left(\frac{j2\pi(\hat{\mathbf{r}}_{rx,n,m}^T \cdot \bar{\mathbf{d}}_{rx,u})}{\lambda_o}\right) \exp\left(\frac{j2\pi(\hat{\mathbf{r}}_{tx,n,m}^T \cdot \bar{\mathbf{d}}_{tx,q})}{\lambda_o}\right) \quad (1)$$

In (1), $\theta_{n,m,ZoD}$ and $\theta_{n,m,ZoA}$ represent the angles of departure (AoD) and arrival (AoA), respectively, in the vertical plane for the m^{th} subpath ($1 \leq m \leq M$) of the n^{th} cluster (corresponding parameters for the horizontal plane are $\phi_{n,m,AoD}$ and $\phi_{n,m,AoA}$, respectively). Moreover, P_n is the power of the n^{th} cluster, set

$\{\Phi_{n,m}^{\theta\theta}, \Phi_{n,m}^{\theta\phi}, \Phi_{n,m}^{\phi\theta}, \Phi_{n,m}^{\phi\phi}\}$ corresponds to initial phases uniformly distributed in $(-\pi, \pi)$ while $\kappa_{n,m}$ parameter is the generated cross polarization power ratio (XPR) for the m^{th} ray of cluster n . In addition, λ_o is the carrier wavelength, $\hat{\mathbf{r}}_{rx,n,m}$ is the spherical unit vector with azimuth arrival angle $\phi_{n,m,AoA}$ and elevation arrival angle $\theta_{n,m,ZoA}$, while $\hat{\mathbf{r}}_{tx,n,m}$ is the spherical unit vector with azimuth departure angle $\phi_{n,m,AoD}$ and elevation departure angle $\theta_{n,m,ZoD}$. Moreover, $F_{tx,q,(\theta \text{ or } \phi)}$ and $F_{rx,u,(\theta \text{ or } \phi)}$ represent the field pattern of transmit/receive antenna element q/u respectively ($1 \leq q \leq N_t$, $1 \leq u \leq N_r$) in the directions of the spherical basis vectors, $\bar{\mathbf{d}}_{rx,u}$ is the location vector of receive antenna element u and $\bar{\mathbf{d}}_{tx,q}$ is the location vector of transmit antenna element q .

Corresponding geometry (considering only the x-y plane) is depicted in Fig. 1, where Ω_{BS}/Ω_{MS} denote the orientation of base station (BS)/MS antenna array, respectively, defined as the difference between the broadside of the BS/MS array and the absolute North (N) reference direction. Moreover, θ_{BS} is the line of sight (LOS) AoD direction between the BS and MS (with respect to the broadside of the BS array), while θ_{MS} is the angle between the BS-MS LOS and the MS broadside. Finally, $\Delta_{n,m,AoD}$ is the angle offset of the m^{th} subpath with respect to $\theta_{n,m,AoD}$ and $\Delta_{n,m,AoA}$ the corresponding offset with respect to $\theta_{n,m,AoA}$.

III. MIMO-5G TRANSCEIVER CONFIGURATION

Considering an arbitrary MIMO configuration with N_t transmitting antennas and N_r receiving antennas ($N_t \times N_r$ system), then the transmitted $N_r \times 1$ signal for the k^{th} MS ($1 \leq k \leq K$, OFDMA transmission is assumed) is given by [14]:

$$\mathbf{x}_k(t) = \left(\frac{1}{S_{sub}} \right) \sum_{l=0}^{\infty} \sum_{s \in \mathcal{U}_k} \sqrt{p_{k,s}} \mathbf{t}_{k,s} X_{k,s,l} e^{j2\pi f_s(t-lT)} \quad (2)$$

where S_{sub} are the available subcarriers, $p_{k,s}$ is the allocated power to the s^{th} subcarrier for the considered MS, T is the duration of the OFDM symbol and $\mathbf{x}_k(t)$, $X_{k,s,l}$ are the transmitted vector signal in time domain and the symbol of the k^{th} MS transmitted from the s^{th} subcarrier at the l^{th} symbol period, respectively. It is assumed that downlink transmission for the k^{th} MS is performed using the subcarriers in set \mathcal{U}_k , with f_s being the corresponding frequency for the s^{th} subcarrier and $\mathbf{t}_{k,s}$ the transmission precoding vector.

The received $N_r \times 1$ signal for each subcarrier resulting after matched filtering and Discrete Fourier Transform (DFT) operation can be expressed as (for simplicity only the first symbol period is considered):

$$\mathbf{y}_{k,s,0} = \left(\sqrt{\frac{p_{k,s}}{TL_{k,sec(k)}}} \right) \mathbf{r}_{k,s} \mathbf{H}_{k,sec(k),s} \mathbf{t}_{k,s} X_{k,s,0} + \sum_{k' \neq k, s \in \mathcal{U}_{k'}} \left(\sqrt{\frac{p_{k',s}}{TL_{k,sec(k')}}} \right) \mathbf{r}_{k,s} \mathbf{H}_{k,sec(k'),s} \mathbf{t}_{k',s} X_{k',s,0} + \mathbf{r}_{k,s} \mathbf{n}_{k,s} \quad (3)$$

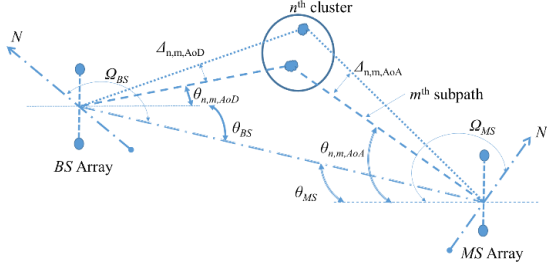


Figure 1. 3GPP channel model for 5G wireless systems

where $\mathbf{H}_{k,sec(k),s}$ is the equivalent channel matrix ($N_r \times N_t$) of the k^{th} MS relevant to its serving sector for the s^{th} subcarrier (each entry is derived after the summation of all cluster components in (1) taking into consideration the corresponding time delays) and TL stands for the total losses (including shadowing and attenuation due to antenna radiation patterns). In particular, pathloss is calculated according to the urban macro-cellular (UMa) model [13]. Moreover, $\mathbf{r}_{k,s} \leftarrow (\mathbf{H}_{k,sec(k),s} \mathbf{t}_{k,s})^H$ is the Maximal Ratio Combining (MRC) multiplying vector [15] and $\mathbf{n}_{k,s}$ the $N_r \times 1$ additive white Gaussian noise.

The corresponding Signal to Interference plus Noise Ratio (SINR) can be expressed as (averaged over a frame duration and assuming that $E(X_k X_{k'}^*) = \delta_{k,k'}$, where $E(x)$ is the mean value of x and δ stands for the Kronecker delta):

$$SINR_{k,s} = \frac{p_{k,s} \mathbf{t}_{k,s}^H \mathbf{H}_{k,sec(k),s}^H \mathbf{r}_{k,s} \mathbf{H}_{k,sec(k),s} \mathbf{t}_{k,s}}{\sum_{k' \neq k, s \in \mathcal{U}_{k'}} \left(\frac{TL_{k,sec(k')}}{TL_{k,sec(k)}} \right) p_{k',s} \mathbf{t}_{k',s}^H \mathbf{H}_{k,sec(k),s}^H \mathbf{r}_{k,s} \mathbf{H}_{k,sec(k),s} \mathbf{t}_{k',s} + \mathbf{r}_{k,s}^H \mathbf{n}_{k,s} \mathbf{r}_{k,s} I_o} \quad (4)$$

where I_o is the thermal noise level. From (3), it follows that the ratio of the desired signal power of a particular MS to the total amount of interference that causes to the rest co-channel MSs (also referred as jamming) can be expressed by (Signal to Jamming Ratio - SJR):

$$SJR_{k,s} = \frac{\mathbf{t}_{k,s}^H \left(\mathbf{H}_{k,sec(k),s}^H \mathbf{H}_{k,sec(k),s} \right) \mathbf{t}_{k,s}}{\mathbf{t}_{k,s}^H \left(\sum_{k' \neq k, s \in \mathcal{U}_{k'}} \mathbf{H}_{k,sec(k),s}^H \mathbf{H}_{k',sec(k),s} \left(\frac{TL_{k,sec(k')}}{TL_{k,sec(k)}} \right) + I_o TL_{k,sec(k)} \right) \mathbf{t}_{k,s}} \quad (5)$$

High SJR values ensure the maximization of the desired MS's signal strength and at the same time the minimization of the interference to the rest of co-channel MSs. Finally, in realistic wireless orientations subcarriers are grouped in PRBs [14], defined as 12 consecutive subcarriers. Therefore, this term will be used throughout this paper to indicate the allocated resource block in frequency domain.

IV. SIMULATION FRAMEWORK

A. Simulation Setup

A hybrid system-link level simulator has been developed, allowing the execution of independent MC simulations in order to evaluate the performance of 5G wireless orientations for various transmission techniques and radio resource management strategies. In this framework, MSs enter the network sequentially in a 5G topology with two tiers of cells around the central cell. For every new MS in the network,

pathloss calculation from all BSs is performed. Afterwards, equivalent channel matrices for all PRBs are generated, according to the channel model described in Section II. In the next step, PRB assignment takes place, based on the proposed approach that will be described in the following subsection. If during power allocation the requested transmission power for acceptable quality of service (QoS) exceeds a predefined threshold, the new (potential) MS is discarded from the network. Otherwise, an MS entry occurs and the simulation terminates when lack of either available power or PRBs is triggered in at least one of the active BSs. The positions of the MSs as well as channel matrices remain constant during an MC run (semistatic simulator). Once the entrance of MSs is finalized, link level simulations take place for a sufficient number of OFDM symbols. Simulation setup and parameter selection are summarized in Table I, aligned with the majority of related works described in [16], regarding system- and link- level simulations.

B. NOMA Grouping Algorithm

The proposed methodology is illustrated in Table II, where $P_{i,b}$ represents the downlink transmission power of the b^{th} BS and $\mathcal{S}_b / \mathcal{S}_{b,NOMA}$ the corresponding set of available/doubly allocated subcarriers per BS, respectively. The latter implies that in this case MS grouping has been performed, whereas a specific subcarrier from this particular set is shared by two MSs. Moreover, $\mathcal{S}_{b,NOMA}^c$ is the complementary set of $\mathcal{S}_{b,NOMA}$. In **Step 2**, the set of available PRBs is defined as a union of the non-allocated PRBs and those which have been allocated only once (i.e., no NOMA transmission has taken place for the specific PRBs). Thereafter, in **Step 3**, PRB s is defined according to the maximization of the product of SINR and SJR for the k^{th} MS. However, if a given PRB has already been assigned to another MS, then the selection criterion is updated accordingly. In this case, NOMA transmission takes place and the set \mathcal{N}_i^c is updated with the indexes of the NOMA MSs (starting with one having the highest SINR), as well as the channel under consideration.

TABLE I. SIMULATION PARAMETERS

Parameter	Value/Assumption
Tiers of cells around the central cell	2
Pathloss model	UMa
Carrier frequency (GHz)	28
Channel Bandwidth (MHz)	100
Cell radius (m)	500
PRBs per BS (N_{PRB}) / Subcarriers per PRB	132/12
Assigned PRBs per MS	5/15
Modulation per PRB / Required E_b/N_o (dB)	QPSK/9.6
Maximum transmission power per BS/MS (P_m/p_m in Table II, units in W)	20/1
Radiation pattern of the antenna element per sector (3 sectors with 120° spatial separation)	Broadside gain = 14 dBi 3dB beamwidth = 70° Front-to-back ratio = 20 dB

In **Step 4**, transmission precoding vector is defined as the eigenvector corresponding to the maximum eigenvalue of matrix $\mathbf{H}_{k,sec(k),s}^H \mathbf{H}_{k,sec(k),s}$ (i.e., $\mathbf{x}(\lambda_m(\mathbf{A}))$ is the eigenvector of matrix \mathbf{A} relative to its maximum eigenvalue). Furthermore, **Step 5** involves the power allocation per PRB. In this case, the Channel Gain (*CG*) per MS and PRB is defined, according to the MSs' channel quality and related total losses (SNR_{th} denotes the minimum Signal to Noise Ratio for acceptable QoS and $|\mathcal{U}_k|$ the number of elements in set \mathcal{U}_k). Finally, in **Step 6**, simulation is finalized either when resource loading (*RL*, defined as the ratio of PRBs that have been assigned to two individual MSs within the same BS to the total available PRBs) exceeds a predefined threshold (denoted as *RLF*) or there is lack of available power in a BS.

In NOMA approach, as depicted in Fig. 2, a specific PRB can be shared by two MSs (denoted as k, k') that are associated with the same BS. In this scenario, the signal of the MS with the highest channel quality is decoded first (denoted as k), treating all other interfering signals as noise. However, for the second MS sharing the same PRB, SIC takes place, where the signal of the k^{th} MS is decoded first and the result is subtracted from the total received signal of the k^{th} MS. The overall procedure is described in the final entries of Table II, where $\zeta_{k',s}$ is the received signal of the k^{th} MS at the s^{th} PRB after MRC processing and $Z_{k',s}$ the corresponding decoded symbol, derived from a set of predefined constellation (denoted as C).

V. RESULTS

In Figs. 3 - 4 the total network throughput and transmission power are presented, respectively, resulting from the proposed NOMA grouping algorithm (mean values have been considered). In this case, a 2×2 MIMO configuration is assumed. All simulation results are depicted in contrast to the tolerable *RLF* that ranges from 10% to 50% (for ease of comparison, OMA transmission is depicted in all simulation scenarios as well). It is assumed that MSs are assigned with either 5 or 15 PRBs (i.e., corresponding transmission rates are 7.2/21.6 Mbps, respectively).

As it can be observed, even for low *RLF* values, a significant throughput gain can be achieved compared to OMA transmission. The throughput gain is more evident for the case of 15 PRBs per MS. In particular, in the OMA case, total throughput is 1573 Mbps. For *RLF* equal to 10%, corresponding value in the NOMA case is 1737 Mbps. Hence, an equivalent throughput gain of almost 11% can be achieved. For *RLF* equal to 20%, the corresponding throughput value is 2131 Mbps, with an equivalent gain of 35% with respect to the OMA case. Moreover, it should be noted that in the first case (i.e., *RLF* equal to 10%), throughput improvement is derived with minimum transmission overhead. In particular, as readily observed in Fig. 4, transmission power in the NOMA/OMA case is 28/26.5 W, respectively. Hence, transmission burden is limited to 5%, i.e., half of the throughput gain. Finally, in Fig. 5 mean BER is illustrated in logarithmic scale considering 15 PRBs per MS and three transceiver scenarios: OMA and NOMA with/without SIC at the receiver.

It should be mentioned that BER is maintained at the corresponding OMA values without employing SIC at the receiver, even for *RLF* equal to 20%. Importantly, these results are particularly promising to drive the design and implementation of realistic 5G networks since simplified transceiver configurations can be employed towards achieving latency-critical applications.

VI. CONCLUSIONS

The performance of a proposed user pairing algorithm in NOMA transmission has been evaluated in the context of 5G networks via a developed hybrid system – link level simulator. According to the presented results, a significant throughput gain can be achieved when NOMA is employed, without any BER deterioration. Future work includes the extension of the developed simulator in order to make the performance evaluation of massive MIMO configurations feasible, thus allowing for future coupling with NOMA transmission.

TABLE II. PROPOSED NOMA MS GROUPING ALGORITHM

<p>Step 1: Set $P_{t,b} \leftarrow 0$, $\mathcal{S}_b \leftarrow \{1:N_{PRB}\}$, $\mathcal{S}_{b,NOMA} \leftarrow \{\}$, ($1 \leq b \leq B$), $l \leftarrow 0$, $k \leftarrow 0$</p> <p>Step 2: $k \leftarrow k+1$. The k^{th} MS tries to access the network in the b^{th} BS requesting R_k PRBs</p> <p style="text-align: center;">Set $\mathcal{S} \leftarrow \mathcal{S}_b \cup \mathcal{S}_{b,NOMA}^c$, $\mathcal{U}_k \leftarrow \{\}$</p> <p>Step 3: $s \leftarrow \underset{s' \in \mathcal{S}}{\text{argmax}} \{SINR_{k,s'} \times SJR_{k,s'}\}$, $\mathcal{S}_b \leftarrow \mathcal{S}_b - s$</p> <p style="text-align: center;">If $s \in \mathcal{U}_{k'}$, with $k' \neq k$, then</p> <p style="text-align: center;">$s \leftarrow \underset{s' \in \mathcal{S}_b}{\text{argmax}} \{SINR_{k',s'} \times SJNR_{k',s'} \times SINR_{k,s} \times SJNR_{k,s'}\}$</p> <p style="text-align: center;">$\mathcal{S}_{b,NOMA} \leftarrow \mathcal{S}_{b,NOMA} \cup s$</p> <p style="text-align: center;">$l \leftarrow l + 1$</p> <p style="text-align: center;">If $SINR_{k,s} > SINR_{k',s}$ then $\mathcal{N}\mathcal{G}_l \leftarrow \{k, k', s\}$</p> <p style="text-align: center;">else $\mathcal{N}\mathcal{G}_l \leftarrow \{k', k, s\}$</p> <p>Step 4: $\mathbf{t}_{k,s} \leftarrow \mathbf{x}(\lambda_m(\mathbf{H}_{k,sec(k),s}^H \mathbf{H}_{k,sec(k),s}))$</p> <p>Step 5: $CG_{k,s} \leftarrow \ \mathbf{H}_{k,sec(k),s} \mathbf{t}_{k,s}\ _F^2 / TL_{k,sec(k)}$, $p_{k,s} \leftarrow (SNR_{th} \cdot I_o) / CG_{k,s}$</p> <p style="text-align: center;">If $p_{k,s} \geq P_m / R_k$ the k^{th} MS is rejected, else</p> <p style="text-align: center;">$\mathcal{S} \leftarrow \mathcal{S}_{b,NOMA}^c \cup \mathcal{S}_b$, $\mathcal{U}_k \leftarrow \mathcal{U}_k \cup s$</p> <p style="text-align: center;">If $\mathcal{U}_k < R_k$ go to step 3</p> <p>Step 6: Set $RL \leftarrow \mathcal{S}_{b,NOMA} / N_{PRB}$, $P_{t,b} \leftarrow P_{t,b} + \sum_{s \in \mathcal{U}_k} p_{k,s}$</p> <p>If $RL \geq RLF$ or $P_{t,b} > P_m$ the MC simulation terminates, else go to Step 2</p> <p>SIC: For every l then $\{k, k', s\} \leftarrow \mathcal{N}\mathcal{G}_l$</p> <p>Decode the s^{th} symbol of the k^{th} MS at the k^{th} receiver (denoted as $Z_{k,s}$). Then:</p> $\zeta_{k',s} \leftarrow \zeta_{k,s} - \left(\sqrt{\frac{p_{k,s}}{TL_{k',sec(k)}}} \right) \mathbf{r}_{k',s} \mathbf{H}_{k',sec(k),s} \mathbf{t}_{k,s} Z_{k,s}$ $Z_{k',s} \leftarrow \underset{y \in C}{\text{argmin}} \zeta_{k',s} - y $
--

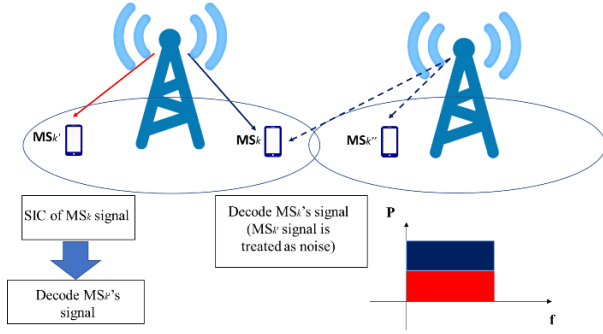


Figure 2. NOMA in cellular networks

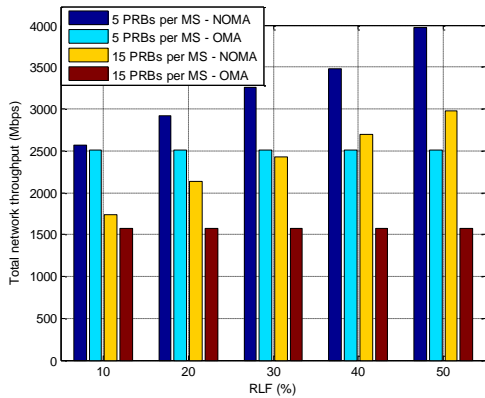


Figure 3. Total network throughput for a 2x2 MIMO configuration

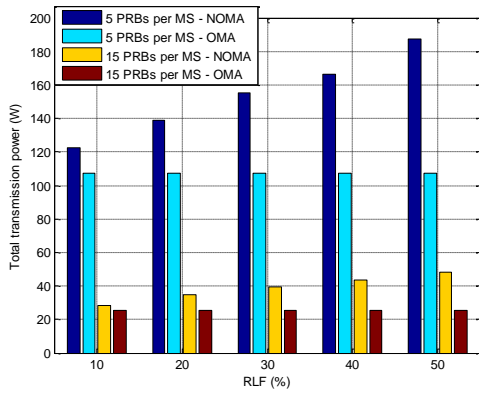


Figure 4. Total transmission power for a 2x2 MIMO configuration

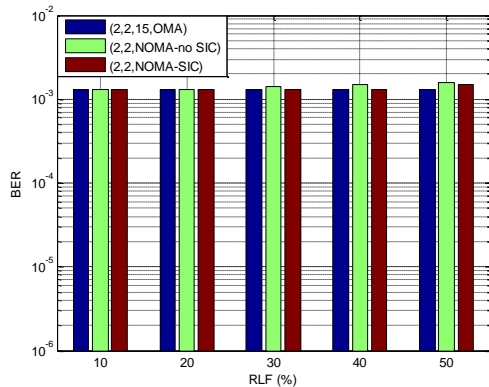


Figure 5. BER for a 2x2 MIMO configuration and 15 PRBs per MS

ACKNOWLEDGMENT

This work has been partially supported by the Affordable5G project, funded by the European Commission under Grant Agreement H2020-ICT-2020-1, number 957317 through the Horizon 2020 and 5G-PPP programs (www.affordable5g.eu/).

REFERENCES

- [1] ITU-R, Report M.2134. Requirements Related to Technical Performance for IMT-Advanced Radio Interface(s), Approved in November 2008.
- [2] G. Naik, S. Bhattarai and J. Park, "Performance Analysis of Uplink Multi-User OFDMA in IEEE 802.11ax," 2018 *IEEE International Conference on Communications (ICC)*, Kansas City, MO, 2018, pp. 1-6, doi: 10.1109/ICC.2018.8422692.
- [3] A. J. Paulraj, D. A. Gore, R. U. Nabar and H. Bolcskei, "An overview of MIMO communications - a key to gigabit wireless," in *Proceedings of the IEEE*, vol. 92, no. 2, pp. 198-218, Feb. 2004, doi: 10.1109/JPROC.2003.821915.
- [4] X. Cheng, C. Tang and Z. Zhang, "Accurate Channel Estimation for Millimeter-Wave MIMO Systems," in *IEEE Transactions on Vehicular Technology*, vol. 68, no. 5, pp. 5159-5163, May 2019, doi: 10.1109/TVT.2019.2905640.
- [5] H. Ji et al., "Overview of Full-Dimension MIMO in LTE-Advanced Pro," *IEEE Communications Magazine*, vol. 55, no. 2, pp. 176-184, February 2017, doi: 10.1109/MCOM.2016.1500743RP.
- [6] L. Dai, B. Wang, Z. Ding, Z. Wang, S. Chen and L. Hanzo, "A Survey of Non-Orthogonal Multiple Access for 5G," *IEEE Communications Surveys & Tutorials*, vol. 20, no. 3, pp. 2294-2323, thirdquarter 2018, doi: 10.1109/COMST.2018.2835558.
- [7] Z. Ding, X. Lei, G. K. Karagiannidis, R. Schober, J. Yuan and V. K. Bhargava, "A Survey on Non-Orthogonal Multiple Access for 5G Networks: Research Challenges and Future Trends," *IEEE Journal on Selected Areas in Communications*, vol. 35, no. 10, pp. 2181-2195, Oct. 2017, doi: 10.1109/JSAC.2017.2725519.
- [8] M. T. P. Le, L. Sanguinetti, E. Björnson and M. D. Benedetto, "What is the Benefit of Code-domain NOMA in Massive MIMO?," *IEEE 30th Annual International Symposium on Personal, Indoor and Mobile Radio Communications (PIMRC)*, Istanbul, Turkey, 2019, pp. 1-5, doi: 10.1109/PIMRC.2019.8904268.
- [9] L. Zhu, J. Zhang, Z. Xiao, X. Cao and D. O. Wu, "Optimal User Pairing for Downlink Non-Orthogonal Multiple Access (NOMA)," *IEEE Wireless Communications Letters*, vol. 8, no. 2, pp. 328-331, April 2019, doi: 10.1109/LWC.2018.2853741.
- [10] Z. Ding, P. Fan and H. V. Poor, "Impact of User Pairing on 5G Nonorthogonal Multiple-Access Downlink Transmissions," *IEEE Transactions on Vehicular Technology*, vol. 65, no. 8, pp. 6010-6023, Aug. 2016, doi: 10.1109/TVT.2015.2480766.
- [11] Y. Ma, T. Lv, X. Li, S. Zhang and W. Guo, "User Pairing Schemes in Cooperative Downlink NOMA System with SWIPT," *Computing, Communications and IoT Applications (ComComAp)*, Shenzhen, China, 2019, pp. 82-87, doi: 10.1109/ComComAp46287.2019.9018780.
- [12] S. Mouchili and S. Hamouda, "Pairing Distance Resolution and Power Control for Massive Connectivity Improvement in NOMA Systems," *IEEE Transactions on Vehicular Technology*, vol. 69, no. 4, pp. 4093-4103, April 2020, doi: 10.1109/TVT.2020.2975539.
- [13] 3GPP TR 38.901 Version 14.3.0 Rel. 14, Study on Channel Model for Frequencies from 0.5 to 100 GHz, 2018.
- [14] 3GPP TS 138 211 Version 15.3.0 Rel.15, 5G NR Physical channels and modulation, 2018.
- [15] A. Goldsmith, *Wireless Communications*, Cambridge University Press, 2005.
- [16] P. K. Gkonis, P.K.; Trakadas and D. I. Kaklamani, "A Comprehensive Study on Simulation Techniques for 5G Networks: State of the Art, Analysis and Future Challenges," *Electronics (MDPI)* 2020, vol. 9, no. 3, doi: 10.3390/electronics9030468.